nature chemical biology

ARTICLE

PUBLISHED ONLINE: 2 MARCH 2015 | DOI: 10.1038/NCHEMBIO.1769

An enzymatic [4+2] cyclization cascade creates the pentacyclic core of pyrroindomycins

Zhenhua Tian[1,5], Peng Sun[1,2,5], Yan Yan[1,5], Zhuhua Wu[1], Qingfei Zheng[1], Shuaixiang Zhou[1], Hua Zhang[1], Futao Yu[1], Xinying Jia[1], Dandan Chen[3], Attila Mándi[4], Tibor Kurtán[4] & Wen Liu[1,3]*

The [4+2] cycloaddition remains one of the most intriguing transformations in synthetic and natural products chemistry. In nature, however, there are remarkably few enzymes known to have this activity. We herein report an unprecedented enzymatic [4+2] cyclization cascade that has a central role in the biosynthesis of pyrroindomycins, which are pentacyclic spirotetramate natural products. Beginning with a linear intermediate that contains two pairs of 1,3-diene and alkene groups, the dedicated cyclases PyrE3 and PyrI4 act in tandem to catalyze the formation of two cyclohexene rings in the dialkyldecalin system and the tetramate spiro-conjugate of the molecules. The two cyclizations are completely enzyme dependent and proceed in a regio- and stereoselective manner to establish the enantiomerically pure pentacyclic core. Analysis of a related spirotetronate pathway confirms that homologs are functionally exchangeable, establishing the generality of these findings and explaining how nature creates diverse active molecules with similar rigid scaffolds.

Pyrroindomycins (PYRs; **Fig. 1a**), which were isolated from *Streptomyces rugosporus* during the screening of agents active against methicillin-resistant *Staphylococcus aureus* and vancomycin-resistant *Enterococcus faecium*[1,2], represent what are to our knowledge the first spirotetramates found in nature. These molecules are structurally related to the spirotetronates chlorothricin (CHL), tetrocarcin A (TC-A), kijanimicin (KIJ) and the lobophorins (LOBs)[3], all of which belong to a large natural product family with two cyclohexene units present in both the dialkyldecalin and the tetramate or tetronate spiro-conjugate portions of the aglycone (**Supplementary Results**, **Supplementary Fig. 1a**). The biosynthetic pathway to establish this characteristic aglycone remains elusive but has been the subject of considerable speculation[4], primarily focusing on whether two sets of 1,3-diene and alkene groups are available in the process for cross-bridging to complete a pentacyclic scaffold via two [4+2] cycloadditions. The [4+2] cycloaddition, in which a 1,3-diene and an alkene react to form a cyclohexene, is one of the classic carbon-carbon bond-forming reactions that is widely used in modern synthetic chemistry. This reaction has long been considered to participate in the biosynthesis of a number of cyclohexene-containing natural products; however, in nature, there are only a few enzymes known to have this activity[5,6]. These enzymes typically exhibit multiple functions, lack catalytic efficiency and/or participate in reactions that proceed spontaneously. Access to their biochemical mechanisms is particularly challenging, leaving unsolved for decades the question of whether an enzyme that catalyzes the Diels-Alder reaction, the quintessential type of [4+2] cycloaddition proceeding through a single pericyclic transition state, naturally occurs[4–8].

Over the past few years, we and others have established the genetic basis for the structural features common in the spirotetramates PYRs and the spirotetronates CHL, TC-A, KIJ and the LOBs[9–13], leading to the hypothesis that these natural products share a similar logic in aglycone biosynthesis (**Fig. 1b**): a modular type I polyketide synthase (PKS) system exclusively programs the assembly of the main carbon skeleton in a linear manner[14–16]. This PKS system has the functional domains, which, colinearly with their activities, are organized in typical modules, and each module contains the indispensable domains ketosynthase (KS), acyltransferase (AT) and acyl carrier protein (ACP) for chain elongation and the optional domains dehydratase (DH), enoylreductase and ketoreductase (KR) for reductively processing β-oxy functionality. There are at least five modules that share the organization KS-AT-DH-KR-ACP, and the resulting ACP-associated oxoacyl intermediate is thus hypothesized to be a polyene polyketide that accordingly has a minimum of five double bonds in its structure (**Fig. 1b**). Elongation of the carbon chain can be terminated by the incorporation of a different three-carbon unit, either an amino acid residue or a glycerate derivative[9,17], to produce the five-membered tetramate or tetronate heterocycle accompanied by off-loading the full-length linear intermediate from the assembly line (**Fig. 1b**). The following modifications most likely involve an acylation-elimination reaction[18], which has recently been characterized in the biosynthesis of the tetronate agglomerin, leading to the generation of an additional double bond that is exocyclic to the five-membered heterocycle (**Fig. 1b**).

Markedly, the six double bonds formed in the proposed biosynthetic pathways of either the spirotetramates PYRs or the spirotetronates CHL, TC-A, KIJ and LOBs constitute two independent pairs of 1,3-diene and alkene groups, the structural hallmarks of the [4+2] cycloaddition reaction (**Fig. 1b**). Taking the locations of the internal and terminal group pairs into account, aglycone biosynthesis is highly anticipated to involve a linear polyketide intermediate that undergoes two [4+2] cycloadditions to establish two cyclohexene-containing portions of the molecule: the dialkyldecalin system and the tetramate or tetronate spiro-conjugate. In this work, we used the PYR biosynthetic machinery as a model system to initiate a search within the encoding clusters for potential cyclases, which would be considered Diels-Alderases if the reactions are concerted, and we eventually confirmed that the two sets of 1,3-diene and alkene groups are indeed present in a polyene polyketide intermediate and, particularly, that the cyclization reactions proceed enzymatically.

[1]State Key Laboratory of Bioorganic and Natural Products Chemistry, Shanghai Institute of Organic Chemistry, Chinese Academy of Sciences, Shanghai, China. [2]Research Center for Marine Drugs, School of Pharmacy, Second Military Medical University, Shanghai, China. [3]Huzhou Center of Bio-Synthetic Innovation, Huzhou, China. [4]Department of Organic Chemistry, University of Debrecen, Debrecen, Hungary. [5]These authors contributed equally to this work. *e-mail: wliu@mail.sioc.ac.cn

RESULTS

Functional assignment of *pyrE3* and *pyrI4* in *pyr* cluster

The search centered on a comparative analysis of the available biosynthetic gene clusters; we first identified the genes for PYRs that are functionally unassigned or difficult to predict and then searched for homologs in other clusters (**Supplementary Fig. 2**). This comparison revealed two candidates in the PYR biosynthetic cluster (*pyr*), *pyrE3* (1,392 bp) and *pyrI4* (555 bp), which respectively code for the proteins PyrE3 and PyrI4 (**Supplementary Figs. 2–4**). PyrE3 belongs to the flavoenzyme superfamily (**Supplementary Fig. 5a**). The members of this family include PgaE and OxyS, which are the flavin adenine dinucleotide (FAD)-dependent hydroxylases that have previously been characterized in the biosynthesis of angucycline and oxytetracycline, respectively[19–21]. In contrast, PyrI4 only shows sequence homology to enzymes with unknown functions (**Supplementary Fig. 5b**). The counterparts of both proteins were found in the pathways of the aforementioned spirotetronates, with ChlE3, TcaE1, LobP3 and KijA being homologous to PyrE3 (46–52% identities) and with ChlL, TcaU4, LobU2 and KijU (**Supplementary Note 2**) being homologous to PyrI4 (26–48% identities), suggesting that they have roles in the construction of certain shared structural features, presumably the dialkyldecalin and the spiro-conjugate moieties. Furthermore, in the gene clusters encoding the spirotetronate metabolites abyssomicin C (ABY-C) and the quartromicins (QMNs), which lack dialkyldecalin structures (**Fig. 1a**), only the genes coding for the PyrI4 counterparts AbyU (29% identity, **Supplementary Note 2**) and QmnH[22,23] are present (**Supplementary Figs. 2** and **4**). Notably, QmnH is 376 amino acids (aa) in length and accordingly harbors two homologs (namely QmnH-N and QmnH-C, respectively), which individually share 24% identity to PyrI4 and 45% identity to each other (**Supplementary Figs. 4** and **5b**). Consequently, PyrI4 is most likely involved in the formation of

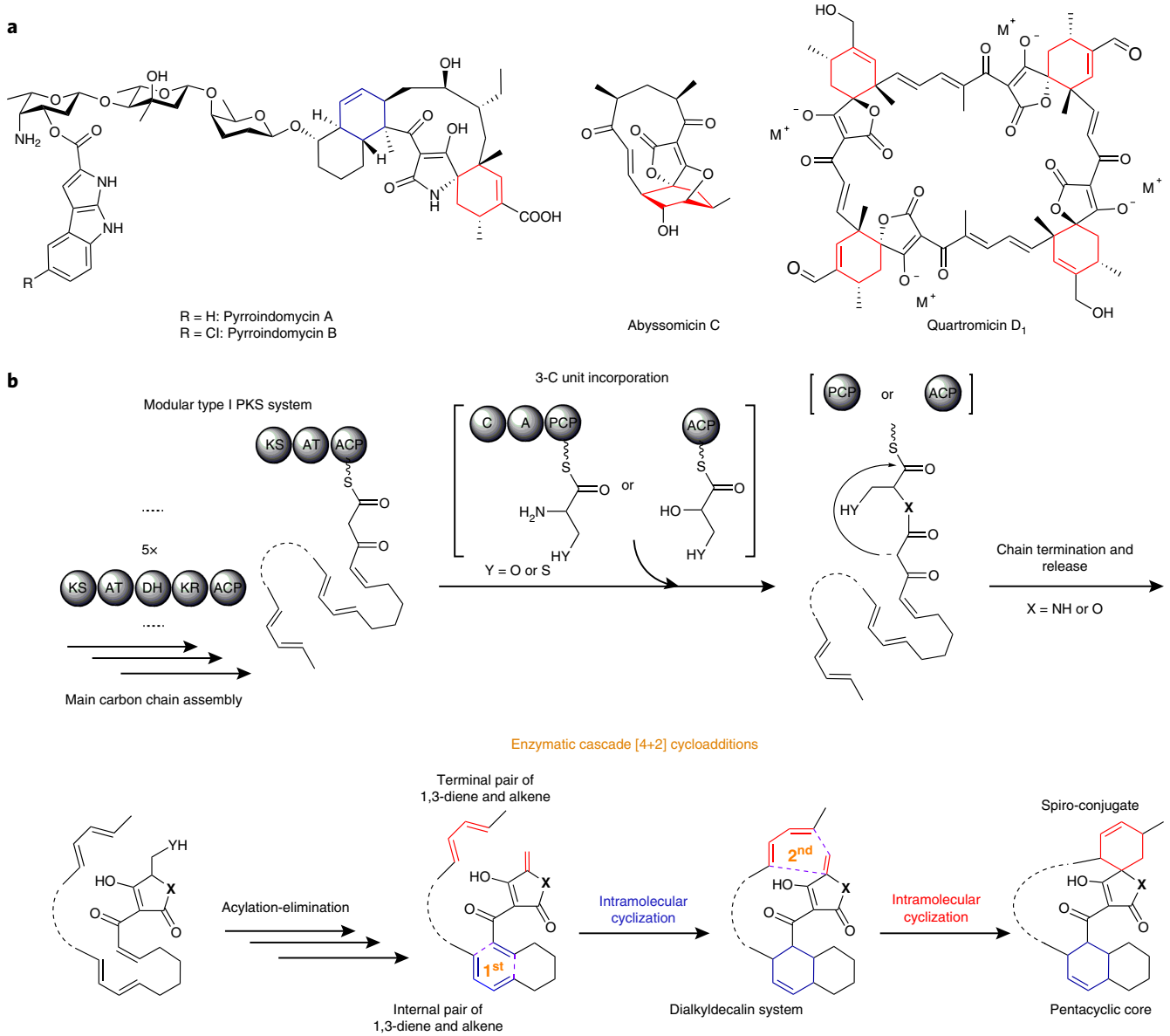

Figure 1 | Spirotetramate and spirotetronate natural products and associated biosynthetic pathway. (**a**) Structures of the spirotetramates, PYRs A and B and the relevant spirotetronates, abyssomicin C (ABY-C) and quartromicin D_1 (QMN- D_1). The cyclohexene units are present in the dialkyldecalin (blue) and/or the spiro-conjugate (red) systems of the molecules. (**b**) Biosynthetic paradigm to establish two sets of 1,3-diene and alkene groups on a linear unsaturated polyketide intermediate for affording the common pentacyclic scaffold through enzymatic cascade [4+2] cycloaddition reactions. The black dashed line indicates the variable linear carbon chain assembled by type I PKSs. The purple dashed line shows the formation of the new carbon-carbon bond. For the two pairs of 1,3-diene and alkene groups, the internal pair is highlighted in blue, and the terminal pair is highlighted in red.

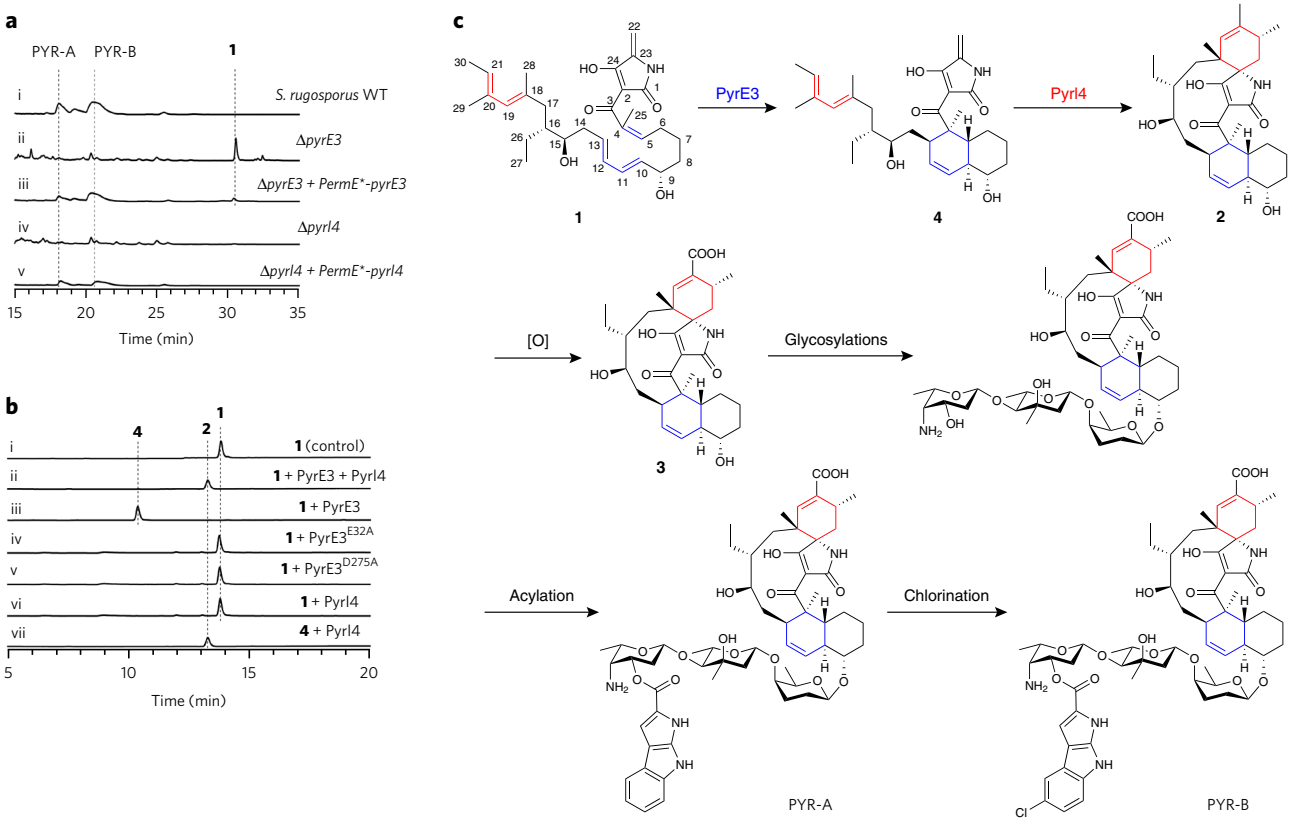

Figure 2 | Characterization of the dialkyldecalin synthase PyrE3 and the spiro-conjugate synthase Pyrl4, which respectively represent two new types of cyclases catalyzing [4+2] cycloaddition reactions. All examinations were performed at least in duplicate (each had at least two parallel samples). (**a**) Production of PYRs and intermediate **1** in the *S. rugosporus* strains. (i) The wild-type (WT) strain. (ii) The Δ*pyrE3* mutant. (iii) The Δ*pyrE3* mutant, in which *pyrE3* is expressed *in trans*. (iv) The Δ*pyrl4* mutant. (v) The Δ*pyrl4* mutant in which *pyrl4* is expressed *in trans*. (**b**) *In vitro* biotransformations catalyzed by PyrE3 and Pyrl4, and each of them alone. (i) Conversion of intermediate **1** in the absence of PyrE3 and Pyrl4; conversions of **1** in the presence of (ii) PyrE3 and Pyrl4, (iii) PyrE3, (iv) the PyrE3^{E32A} mutant, (v) the PyrE3^{D275A} mutant and (vi) Pyrl4; and (vii) conversion of intermediate **4** in the presence of Pyrl4. (**c**) Individual roles of PyrE3 and Pyrl4 in the biosynthetic pathway of PYRs. PyrE3-catalyzed dialkyldecalin formation is shown in blue, and Pyrl4-catalyzed spiro-conjugate formation is shown in red.

the more common spiro-conjugate, leaving PyrE3 responsible for the construction of the dialkyldecalin.

Characterization of the linear PYR intermediate

To confirm the functional assignment of *pyrE3* and *pyrI4*, we individually inactivated these genes in wild-type *S. rugosporus* (**Fig. 2**). Both the Δ*pyrE3* and Δ*pyrI4* mutant strains lost the ability to produce PYRs, which was partially restored by *in trans* complementation of the corresponding gene (**Fig. 2a**). Thus, the involvement of PyrE3 and PyrI4 in PYR biosynthesis was established. Although the inactivation of *pyrI4* did not apparently lead to the accumulation of a new product, intermediate **1** was detected upon the inactivation of *pyrE3* (**Fig. 2a**). We then fermented the Δ*pyrE3* mutant strain on a large scale and accumulated a sufficient quantity of **1** for structural elucidation. NMR and MS analyses revealed that **1** is a 30-carbon linear polyene polyketide (**Fig. 2c** and **Supplementary Note 3**). Overall, the structure of **1** is consistent with the proposed PYR biosynthetic logic[9], which was previously established according to an analysis of the functional domains of the PKSs for building block selection and incorporation and particularly for reductive β-oxo processing to control the stereochemical configurations of the corresponding functionalities (**Supplementary Fig. 6**)[24–28]. Amino acid incorporation and modification clearly precede the formation of the dialkyldecalin in PYR biosynthesis because **1** is linear and terminates with a mature γ-methylene-tetramate unit (**Fig. 2c**). Notably, **1** simultaneously bears two unsaturated systems, with the internal pair, $\Delta^{4,5}$-alkene and $\Delta^{10,11}$, $\Delta^{12,13}$-diene, corresponding to the dialkyldecalin and the terminal pair, $\Delta^{22,23}$-methylene and $\Delta^{18,19}$, $\Delta^{20,21}$-diene, corresponding to the tetramate spiro-conjugate. This finding strongly supports the feasibility of two cascade [4+2] cycloadditions, for which we provide structural evidence for what is to our knowledge the first time (**Fig. 1b**). Intermediate **1** was relatively stable in aqueous solution as no transformation was detected at room temperature over a 24-h incubation period. This stability greatly facilitated the characterization of the cyclization reactions, including their enzyme dependence and regio- and stereoselectivity.

Enzymatic construction of the pentacyclic core of PYRs

We expressed and purified PyrE3 and PyrI4 from *Escherichia coli* (**Supplementary Fig. 7a**) and then assayed their activities *in vitro*. In the presence of both proteins, the linear intermediate **1** was rapidly converted into a sole product, **2**, and required no addition of exogenous cofactors such as FAD^+, $FADH_2$, $NAD(P)^+$, NAD(P)H or various metal ions (**Fig. 2b**). This conversion was scaled up, leading to the characterization of **2** as a highly rigidified pentacyclic compound (**Fig. 2c** and **Supplementary Note 3**). Remarkably, **2** has the two intact cyclohexene-containing systems characteristic of PYRs, i.e., the dialkyldecalin and the tetramate spiro-conjugate, unambiguously demonstrating that enzymatic coordination is necessary for multiple cross-bridging of **1**.

Although PYRs were reported in 1994 (refs. 1,2), the stereochemistry of the central aglycone has not yet been established. We therefore fermented the *S. rugosporus* wild-type strain, from which PYRs were isolated, followed by hydrolysis to remove the

Table 1 | Steady-state kinetic parameters of enzymatic [4+2] cycloaddition reactions.

Protein	Substrate	K_m (μM)	k_{cat} (min^{-1})	k_{cat}/K_m ($\mu M^{-1}\ min^{-1}$)
PyrE3	**1**	51.5 ± 2.3	223.2 ± 5.4	4.3
PyrI4	**4**	224.0 ± 3.5	342.6 ± 3.3	3.1
ChlE3	**1**	163.4 ± 6.1	5.2 ± 0.4	0.03
ChlL	**4**	327.5 ± 12.4	1.5 ± 0.05	0.005

The catalysts include PyrE3 and ChlE3 for dialkyldecalin formation and PyrI4 and ChlL for spiro-conjugate formation. All values are ± s.e.m.

pyrroloindole-substituted deoxytrisaccharide side chain. These efforts produced the natural aglycone **3** (**Fig. 2c**) for structural comparison with the enzymatic product **2**. Product **2** was extremely similar to **3** according to the spectral data (**Supplementary Note 3**), indicating their stereochemical identity. Consequently, the formation of the enantiomerically pure pentacyclic scaffold completely depends on the enzymatic activities of PyrE3 and PyrI4. The only difference between product **2** and aglycone **3** was found at C20, which is substituted with a methyl group in **2** rather than a carboxyl group in **3**, providing the evidence that **2** serves as the precursor of **3** and that the C20 methyl group is processed through a six-electron oxidation (**Fig. 2c**). The attachment of the sugar side chain at C9 followed by the transfer of the pyrroloindolic moiety could result in the final products PYR-A and PYR-B, depending on the absence or presence of the additional chlorination step.

The assigned structure of **3** and its deduced relative configuration (4*R**, 5*R**, 9*S**, 10*S**, 13*R**, 15*R**, 16*R**, 18*R**, 21*R**, 23*S**) were confirmed by single-crystal X-ray diffraction analysis using Mo Kα radiation (**Supplementary Note 3** and **Supplementary Data Set 1**). Clearly, the dialkyldecalin is an *endo* product, in contrast to the tetramate spiro-conjugate, which is an *exo* adduct. Furthermore, density functional theory (DFT) analysis and time-dependent DFT (TDDFT)-electronic CD (ECD) calculations (with the experimental ECD spectrum for comparison) were conducted to establish the absolute configuration of **3** (**Fig. 2c**). These analyses revealed the preferred solution conformations and the conformational rigidity of the 11-membered central ring (**Supplementary Note 3**).

Validation of PyrE3 as a FAD-dependent [4+2] cyclase

We investigated the individual roles of PyrE3 and PyrI4 in the conversion of **1** to **2**. Intermediate **1** was incubated with either PyrE3 or PyrI4 alone (**Fig. 2b**). Although no reaction occurred in the presence of PyrI4, PyrE3 converted **1** exclusively into **4** (**Fig. 2c**), again in the absence of any added cofactors. Compared with substrate **1** and product **2**, **4** is a partially cyclized intermediate (**Supplementary Note 3**). This compound bears the intact dialkyldecalin system, which, identically to that in **2**, replaces the corresponding internal pair of $\Delta^{4,5}$-alkene and $\Delta^{10,11}$, $\Delta^{12,13}$-diene in **1**. However, similar to **1**, **4** retains the free terminal pair of $\Delta^{22,23}$-methylene and $\Delta^{18,19}$, $\Delta^{20,21}$-diene. Thus, PyrE3 is a dedicated dialkyldecalin synthase that catalyzes the first intramolecular [4+2] cyclization to afford the cyclohexene adduct (**Fig. 2c**). This reaction proceeded with a moderate efficiency, as indicated by the observed steady-state kinetic parameters (**Table 1** and **Supplementary Fig. 8**).

The recombinant PyrE3 protein purified from *E. coli* appeared light yellow in color and exhibited an absorbance spectrum characteristic of a flavoprotein containing the flavin cofactor in oxidized form (**Supplementary Fig. 7b**). PyrE3 binds the cofactor in a non-covalent manner, thus permitting its release by heating for high-resolution ESI-MS analysis, which confirmed the identity as FAD. PyrE3 is phylogenetically similar to a large number of FAD-binding proteins with variable redox-relevant activities (**Supplementary Fig. 5a**), for which NAD(P)H and $NAD(P)^+$ are often required to regenerate FAD or its reduced form, $FADH_2$. PyrE3-catalyzed cyclization is independent of an NAD(P) cofactor, suggesting that the flavin cofactor does not cycle between oxidized and reduced forms and that it therefore does not have a typical redox role in the reaction. The crystal structure of OxyS (41% identity to PyrE3)[21], the FAD-dependent hydroxylase in oxytetracycline biosynthesis, was selected for homology modeling, leading to the identification of the residues E32 and D275 in PyrE3, which are potentially essential for FAD binding. We conducted site-specific mutation of these two residues, and the resulting mutant proteins, $PyrE3^{E32A}$ and $PyrE3^{D275A}$, were colorless, as expected (**Supplementary Fig. 7b**). $PyrE3^{E32A}$ and $PyrE3^{D275A}$ failed to convert **1** (**Fig. 2b**), validating the FAD dependence of PyrE3 activity. Consequently, PyrE3 may have evolved from an ancestor binding FAD. In light of the increasing precedents for flavoenzymes to catalyze reactions in the absence of a change in redox state of the cofactor[29], it seems that the FAD of PyrE3 has a structural role in maintaining the requisite geometry of the active site for the [4+2] cycloaddition. To support this hypothesis, we examined the ECD spectra of the native and mutant PyrE3 proteins (**Supplementary Fig. 7b**). The spectra of $PyrE3^{E32A}$ and $PyrE3^{D275A}$ were highly similar to each other but clearly distinct from that of the native PyrE3, indicating a remarkable difference in protein structure that arises from the absence and presence of FAD.

Validation of PyrI4 as a spiro-conjugate synthase

Like **1**, intermediate **4** was relatively stable in aqueous solution. During incubation at room temperature (~25 °C) over a 24-h period, this compound was incapable of undergoing a spontaneous transformation into product **2**, indicating that the cycloaddition of the terminal $\Delta^{22,23}$-methylene and $\Delta^{18,19}$, $\Delta^{20,21}$-diene depends on additional enzymatic activity. Indeed, the conversion of **4** to **2** only occurred in the presence of PyrI4 and without any other byproducts (**Fig. 2b**), thus validating the idea that PyrI4 is a specific spiro-conjugate synthase responsible for the second intramolecular [4+2] cyclization to complete the pentacyclic core (**Fig. 2c**). This reaction was metal ion independent and proceeded moderately, consistent with its observed steady-state kinetic parameters (**Table 1** and **Supplementary Fig. 8**). PyrI4 was unable to act on linear intermediate **1**, confirming that its activity relies on the formation of the dialkyldecalin adduct.

Generality evaluation for pentacyclic core formation

We subsequently evaluated the generality of the newly characterized enzymatic cascade [4+2] cycloadditions in the biosynthesis of CHL (**Fig. 3**), a spirotetronate natural product that is structurally related to PYRs[10]. Individual inactivation of *chlE3* (the homolog of *pyrE3*, 52% identity) and *chlL* (the homolog of *pyrI4*, 48% identity) in the wild-type *S. antibioticus* strain completely abolished CHL production, confirming their necessity for CHL biosynthesis (**Fig. 3a**). Remarkably, heterologous complementation of *pyrE3* or *pyrI4*, the homolog in PYR biosynthesis, to the corresponding *S. antibioticus* Δ*chlE3* or Δ*chlL* mutant strain partially restored the production of CHL (**Fig. 3a**). A similar result was found in the *S. rugosporus* Δ*pyrE3* or Δ*pyrI4* mutant strain, in which the heterologous expression of *chlE3* or *chlL* led to the production of PYRs (**Fig. 3b**). Clearly, the *chlE3* and *chlL* genes are functionally exchangeable with *pyrE3* and *pyrI4*, respectively.

The products of these genes, ChlE3 and ChlL, were then expressed and purified to convert PYR intermediate **1** *in vitro* (**Supplementary Fig. 7a**). Although kinetically less efficient than PyrE3 and PyrI4 (**Table 1**, **Fig. 3c** and **Supplementary Figs. 8** and **9**), both proteins were active in a highly ordered process, as ChlE3 catalyzed the conversion of **1** into the partially cyclized intermediate **4**, which was then transformed by ChlL into the fully cyclized product **2**. During each of the catalytic processes, no byproducts, including any isomer of the product, were found, indicating that

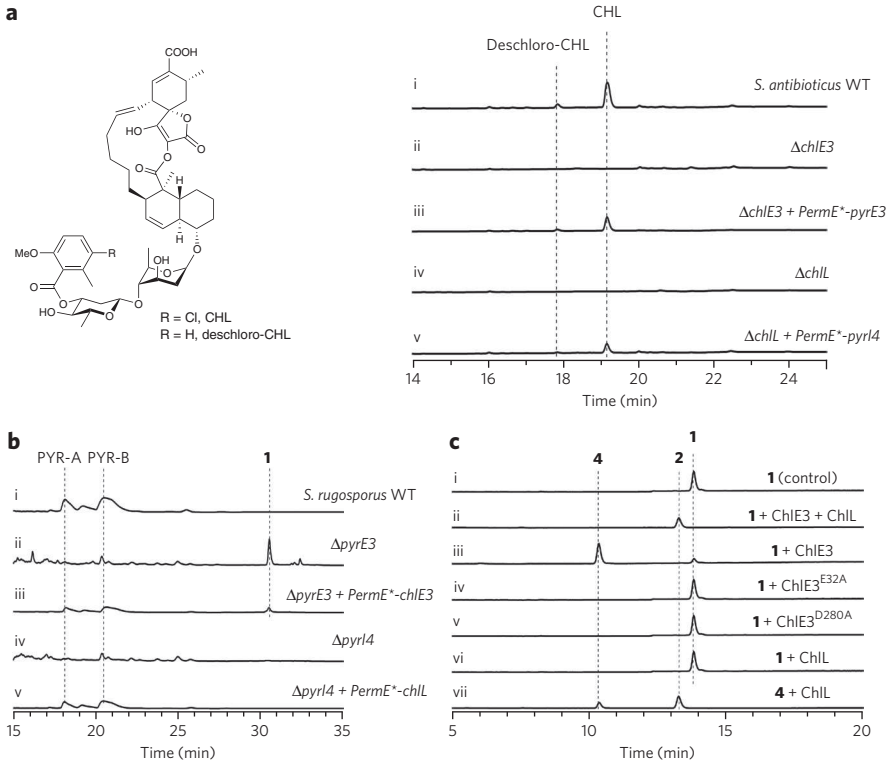

Figure 3 | Validation of the functional identity of ChlE3 and ChlL to PyrE3 and PyrI4, respectively. All examinations were performed at least in duplicate (each had at least two parallel samples). (**a**) Structures of CHL and deschloro-CHL (left) and their production in the *S. antibioticus* strains (right). (i) The wild-type (WT) CHL-producing strain. (ii) The Δ*chlE3* mutant. (iii) The Δ*chlE3* mutant in which *pyrE3* is heterologously expressed *in trans*. (iv) The Δ*chlL* mutant. (v) The Δ*chlL* mutant in which *pyrI4* is heterologously expressed *in trans*. Deschloro-CHL, an intermediate previously characterized in the CHL biosynthetic pathway[10], is often produced together with CHL in fermentation. (**b**) Production of PYRs in the *S. rugosporus* strains. (i) The wild-type PYRs-producing strain. (ii) The Δ*pyrE3* mutant. (iii) The Δ*pyrE3* mutant in which *chlE3* is heterologously expressed *in trans*. (iv) The Δ*pyrI4* mutant. (v) The Δ*pyrI4* mutant in which *chlL* is heterologously expressed *in trans*. (**c**) *In vitro* biotransformations catalyzed by ChlE3 and ChlL and by each of them alone. (i) Conversion of intermediate **1** of PYRs in the absence of ChlE3 and ChlL; conversions of **1** in the presence of (ii) ChlE3 and ChlL, (iii) ChlE3, (iv) the ChlE3^{E32A} mutant, (v) the ChlE3^{D280A} mutant and (vi) ChlL; and (vii) conversion of intermediate **4** in the presence of ChlL.

ChlE3 and ChlL are equivalent to PyrE3 and PyrI4 in the control of regio- and stereoselectivity. Similarly to PyrE3, ChlE3 is a flavoenzyme that binds FAD, and mutations at the FAD-binding site produced the proteins ChlE3^{E32A} and ChlE3^{D280A}, which were colorless, inactive and markedly changed in the ECD spectrum (**Fig. 3c** and **Supplementary Fig. 7c**). Together, these findings support the hypothesis that the CHL and PYR biosynthetic pathways share a multiple cross-bridging strategy to construct the pentacyclic core via two [4+2] cyclizations that occur in tandem (**Supplementary Fig. 10**), despite differences in their linear polyene substrates, which vary in length, substitution pattern and whether they contain tetronate or tetramate functionalities[9,10].

DISCUSSION

In this study, we have uncovered a common paradigm for the biosynthesis of both spirotetramate natural products (PYRs) and spirotetronate (CHL), in which the enzymatic [4+2] cyclization cascade has a central role in the formation of the highly rigid pentacyclic core by coordinated cross-bridging of a linear polyene intermediate (**Fig. 1c**). We characterized two new types of [4+2] cyclases in this enantioselectively pure biotransformation (**Fig. 2c**): a dialkyldecalin synthase, represented by PyrE3 or ChlE3, and a spiro-conjugate synthase, represented by PyrI4 or ChlL. Very recently, VstJ[30], which shares the sequence homology to PyrI4 (26% identity) and ChlL (24% identity), was characterized in the biosynthesis of the structurally related spirotetronate, versipelostatin (**Supplementary Fig. 1a**). These proteins are functionally identical, thereby supporting the generality for spiro-conjugate formation via [4+2] cycloaddition. Both types of proteins are monofunctional and catalyze the pure enzymatic cyclizations, in contrast to the rather few enzymes that were previously shown to catalyze [4+2] cyclizations[5], including the multifunctional catalysts macrophomate synthase[31], solanapyrone synthase (Sol5)[32], lovastatin synthase (LovB)[33,34] and riboflavin synthase[35] as well as the recently characterized, standalone cyclase in spinosyn biosynthesis[36], SpnF (**Fig. 4**). In the majority of these examples, the corresponding cyclizations can occur spontaneously.

It is worth considering the possibility that concerted Diels-Alder cyclization is operative in the two reactions catalyzed by PyrE3 or ChlE3 and by PyrI4 or ChlL (for each of which the stereochemical outcome is consistent with the Woodward-Hoffmann rules concerning this type of [4+2] cycloadditions[37]), although other mechanisms, such as a polar stepwise addition, cannot be excluded at this time. In fact, the Diels-Alder reaction has been widely used in the chemical synthesis of spirotetronate aglycones to assemble both the dialkyldecalin and spiro-conjugate systems[38,39]. Whether the biosynthetic pathway imitates the synthetic route is of particular interest, and if it does, the dialkyldecalin formation would undergo an *endo*-selective Diels-Alder reaction, whereas the spiro-conjugate formation would follow an *exo*-transition state. A number of microorganisms, including those that biosynthesize as-yet-unidentified metabolites, harbor genes coding for PyrI4- or ChlL-like spiro-conjugate synthases and either have or do not have genes encoding PyrE3- or ChlE3-like dialkyldecalin synthases in the respective gene clusters (**Supplementary Fig. 5**), suggesting that the coupling (for example, for PYRs, CHL, TC-A, KIJ and LOBs) or uncoupling (for example, for ABY-C and QMNs) of the two associated enzymatic [4+2] cycloadditions is a common strategy used in nature to produce diverse active molecules with similar rigid scaffolds (**Supplementary Fig. 1**).

Notably, all known types of [4+2] cyclases are phylogenetically distinct (**Fig. 4**): even though the products share a similar 6,6-bicyclic moiety, the dialkyldecalin synthases represented by PyrE3 and ChlE3 in the PYR and CHL biosynthetic pathways share no homology with other relevant types of [4+2] cyclases, such as LovB in lovastatin biosynthesis and Sol5 in solanapyrone biosynthesis. We thus hypothesize that these [4+2] cyclases associated with the

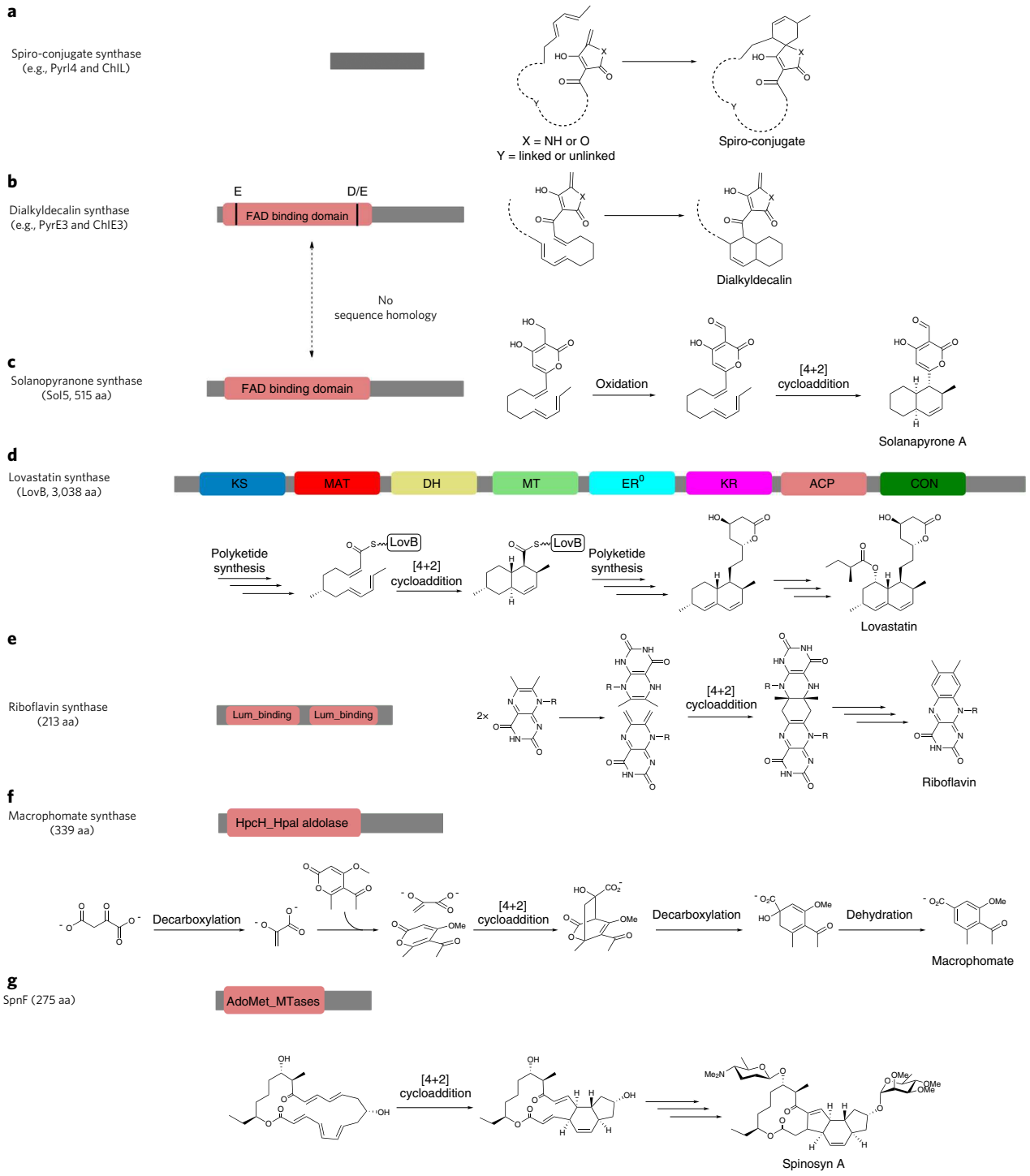

Figure 4 | Known (putative) types of [4+2] cyclases and associated conversions in the pathways. The sizes of enzymes and their conserved domain organizations are compared here and shown in color. For the reactions, the overall structures of the 1,3-diene and alkene-containing precursors and the cyclohexene-containing products are shown. (**a**,**b**) For spiro-conjugate synthase (**a**) and dialkyldecalin synthase (**b**), dashed lines indicate the variable side chains, which can be coupled for intramolecular cyclization (for example, for PYRs and CHL) or uncoupled for intermolecular cyclization (for example, for QMNs). (**c**) Solanapyrone synthase Sal5 has no sequence homology to either PyrE3 or ChlE3, although they potentially share FAD-binding ability. (**d**) LovB domains. MAT, malonyl-CoA acyltransferase; MT, methyltransferase; ER^0, inactive enoylreductase; CON, condensation protein. (**e**) Riboflavin synthase contains two domains for binding of the substrate lumazine. (**f**) Macrophomate synthase phylogenetically belongs to an aldolase family. (**g**) SpnF shares sequence similarity with various *S*-adenosyl-L-methionine (AdoMet)-dependent methyltransferases (MTases).

pathways of diverse natural products have evolved independently from different proteins. The enzymatic activity for [4+2] cyclization, similar to that recently characterized for spiroketal biosynthesis[40,41], may result from the close interaction between ancestral proteins and diverse 1,3-diene and alkene-containing substrates, toward cross-bridging to form the cyclohexene unit in the structure. This natural co-evolution of protein and chemical structure could be intrinsic for enzymatic [4+2] cycloadditions, including Diels-Alder

reactions, in which the enzyme has been suggested as an 'entropic trap'[4–8], creating a number of phylogenetically distinct but functionally identical [4+2] cyclases for accommodating the 1,3-diene and alkene groups of different substrates in the biosynthesis of diverse cyclohexene-containing natural products.

Received 1 December 2014; accepted 4 February 2015; published online 2 March 2015

METHODS

Methods and any associated references are available in the online version of the paper.

Accession codes. Cambridge Crystallographic Data Centre. The crystal structure of 3 is deposited under accession number CCDC 1046624.

References

1. Ding, W. *et al.* Pyrroindomycins, novel antibiotics produced by *Streptomyces rugosporus* sp. LL-42D005. I. Isolation and structure determination. *J. Antibiot. (Tokyo)* **47**, 1250–1257 (1994).
2. Singh, M.P. *et al.* Pyrroindomycins, novel antibiotics produced by *Streptomyces rugosporus* LL-42D005. II. Biological activities. *J. Antibiot. (Tokyo)* **47**, 1258–1265 (1994).
3. Vieweg, L., Reichau, S., Schobert, R., Leadlay, P.F. & Sussmuth, R.D. Recent advances in the field of bioactive tetronates. *Nat. Prod. Rep.* **31**, 1554–1584 (2014).
4. Oikawa, H. & Tokiwano, T. Enzymatic catalysis of the Diels-Alder reaction in the biosynthesis of natural products. *Nat. Prod. Rep.* **21**, 321–352 (2004).
5. Kim, H.J., Ruszczycky, M.W. & Liu, H.W. Current developments and challenges in the search for a naturally selected Diels-Alderase. *Curr. Opin. Chem. Biol.* **16**, 124–131 (2012).
6. Kelly, W.L. Intramolecular cyclizations of polyketide biosynthesis: mining for a "Diels-Alderase"? *Org. Biomol. Chem.* **6**, 4483–4493 (2008).
7. Townsend, C.A.A. "Diels-Alderase" at last. *ChemBioChem* **12**, 2267–2269 (2011).
8. Kelly, W.L. Biochemistry: life imitates art. *Nature* **473**, 35–36 (2011).
9. Wu, Q., Wu, Z., Qu, X. & Liu, W. Insights into pyrroindomycin biosynthesis reveal a uniform paradigm for tetramate/tetronate formation. *J. Am. Chem. Soc.* **134**, 17342–17345 (2012).
10. Jia, X.Y. *et al.* Genetic characterization of the chlorothricin gene cluster as a model for spirotetronate antibiotic biosynthesis. *Chem. Biol.* **13**, 575–585 (2006).
11. Fang, J. *et al.* Cloning and characterization of the tetrocarcin A gene cluster from *Micromonospora chalcea* NRRL 11289 reveals a highly conserved strategy for tetronate biosynthesis in spirotetronate antibiotics. *J. Bacteriol.* **190**, 6014–6025 (2008).
12. Zhang, H. *et al.* Elucidation of the kijanimicin gene cluster: insights into the biosynthesis of spirotetronate antibiotics and nitrosugars. *J. Am. Chem. Soc.* **129**, 14670–14683 (2007).
13. Li, S. *et al.* Dissecting glycosylation steps in lobophorin biosynthesis implies an iterative glycosyltransferase. *Org. Lett.* **15**, 1374–1377 (2013).
14. Staunton, J. & Weissman, K.J. Polyketide biosynthesis: a millennium review. *Nat. Prod. Rep.* **18**, 380–416 (2001).
15. Walsh, C.T. Polyketide and nonribosomal peptide antibiotics: modularity and versatility. *Science* **303**, 1805–1810 (2004).
16. Weissman, K.J. & Leadlay, P.F. Combinatorial biosynthesis of reduced polyketides. *Nat. Rev. Microbiol.* **3**, 925–936 (2005).
17. Sun, Y. *et al. In vitro* reconstruction of tetronate RK-682 biosynthesis. *Nat. Chem. Biol.* **6**, 99–101 (2010).
18. Kanchanabanca, C. *et al.* Unusual acetylation-elimination in the formation of tetronate antibiotics. *Angew. Chem. Int. Ed. Engl.* **52**, 5785–5788 (2013).
19. Koskiniemi, H. *et al.* Crystal structures of two aromatic hydroxylases involved in the early tailoring steps of angucycline biosynthesis. *J. Mol. Biol.* **372**, 633–648 (2007).
20. Kallio, P. *et al.* Tracing the evolution of angucyclinone monooxygenases: structural determinants for C-12b hydroxylation and substrate inhibition in PgaE. *Biochemistry* **52**, 4507–4516 (2013).
21. Wang, P. *et al.* Uncovering the enzymes that catalyze the final steps in oxytetracycline biosynthesis. *J. Am. Chem. Soc.* **135**, 7138–7141 (2013).
22. Gottardi, E.M. *et al.* Abyssomicin biosynthesis: formation of an unusual polyketide, antibiotic-feeding studies and genetic analysis. *ChemBioChem* **12**, 1401–1410 (2011).
23. He, H.Y. *et al.* Quartromicin biosynthesis: two alternative polyketide chains produced by one polyketide synthase assembly line. *Chem. Biol.* **19**, 1313–1323 (2012).
24. Bisang, C. *et al.* A chain initiation factor common to both modular and aromatic polyketide synthases. *Nature* **401**, 502–505 (1999).
25. Reeves, C.D. *et al.* Alteration of the substrate specificity of a modular polyketide synthase acyltransferase domain through site-specific mutations. *Biochemistry* **40**, 15464–15470 (2001).
26. Keatinge-Clay, A.T. A tylosin ketoreductase reveals how chirality is determined in polyketides. *Chem. Biol.* **14**, 898–908 (2007).
27. Wu, J., Zaleski, T.J., Valenzano, C., Khosla, C. & Cane, D.E. Polyketide double bond biosynthesis. Mechanistic analysis of the dehydratase-containing module 2 of the picromycin/methylmycin synthase. *J. Am. Chem. Soc.* **127**, 17393–17404 (2005).
28. Kwan, D.H. *et al.* Prediction and manipulation of the stereochemistry of enoylreduction in modular polyketide synthases. *Chem. Biol.* **15**, 1231–1240 (2008).
29. Bornemann, S. Flavoenzymes that catalyse reactions with no net redox change. *Nat. Prod. Rep.* **19**, 761–772 (2002).
30. Hashimoto, T. *et al.* Biosynthesis of versipelostatin: identification of an enzyme-catalyzed [4+2]-cycloaddition required for macrocyclization of spirotetronate-containing polyketides. *J. Am. Chem. Soc.* **137**, 572–575 (2015).
31. Ose, T. *et al.* Insight into a natural Diels-Alder reaction from the structure of macrophomate synthase. *Nature* **422**, 185–189 (2003).
32. Oikawa, H., Katayama, K., Suzuki, Y. & Ichihara, A. Enzymatic activity catalysing exo-selective Diels-Alder reaction in solanapyrone biosynthesis. *J. Chem. Soc. Chem. Commun.*##1321–1322 (1995).
33. Auclair, K. *et al.* Lovastatin nonaketide synthase catalyzes an intramolecular Diels-Alder reaction of a substrate analogue. *J. Am. Chem. Soc.* **122**, 11519–11520 (2000).
34. Ma, S.M. *et al.* Complete reconstitution of a highly reducing iterative polyketide synthase. *Science* **326**, 589–592 (2009).
35. Kim, R.R. *et al.* Mechanistic insights on riboflavin synthase inspired by selective binding of the 6,7-dimethyl-8-ribityllumazine exomethylene anion. *J. Am. Chem. Soc.* **132**, 2983–2990 (2010).
36. Kim, H.J., Ruszczycky, M.W., Choi, S.H., Liu, Y.N. & Liu, H.W. Enzyme-catalysed [4+2] cycloaddition is a key step in the biosynthesis of spinosyn A. *Nature* **473**, 109–112 (2011).
37. Carey, F.A. in *Organic Chemistry* 4th edn. 365–397 (Mcgraw-Hill Higher Education, New York, 2000).
38. Roush, W.R., Reilly, M.L., Koyama, K. & Brown, B.B. A formal total synthesis of (+)-tetronolide, the aglycon of the tetrocarcins: enantio-and diastereoselective syntheses of the octahydronaphthalene (bottom-half) and spirotetronate (top-half) fragments. *J. Org. Chem.* **62**, 8708–8721 (1997).
39. Roush, W.R. & Sciotti, R.J. Enantioselective total synthesis of (−)-chlorothricolide via the tandem inter- and intramolecular Diels–Alder reaction of a hexaenoate intermediate. *J. Am. Chem. Soc.* **120**, 7411–7419 (1998).
40. Takahashi, S. *et al.* Reveromycin A biosynthesis uses RevG and RevJ for stereospecific spiroacetal formation. *Nat. Chem. Biol.* **7**, 461–468 (2011).
41. Sun, P. *et al.* Spiroketal formation and modification in avermectin biosynthesis involves a dual activity of AveC. *J. Am. Chem. Soc.* **135**, 1540–1548 (2013).

Acknowledgments

This work was supported in part by grants from the National Natural Science Foundation of China (91213303, 81202453, 31430005 and 91413101), STCSM (14JC1407700 and 13XD1404500), the Ministry of Science and Technology of China (2012AA02A706) and the National Research Foundation (OTKA K105871) of Hungary.

Author contributions

Z.T., Z.W., H.Z., X.J. and D.C. performed the *in vivo* investigations. Z.T., Y.Y., S.Z., F.Y. and Q.Z. conducted the *in vitro* enzymatic investigations. P.S., Y.Y. and Z.W. characterized the chemical compounds. A.M. and T.K. conducted the DFT conformational analysis and TDDFT-ECD calculation. Z.T. performed the sequence analysis. Z.T., P.S. and W.L. analyzed the data and wrote the manuscript. W.L. directed the research.

Competing financial interests

The authors declare no competing financial interests.

Additional information

Supplementary information and chemical compound information is available in the online version of the paper. Reprints and permissions information is available online at http://www.nature.com/reprints/index.html. Correspondence and requests for materials should be addressed to W.L.

ONLINE METHODS

Materials, bacterial strains and plasmids. Biochemicals and media were purchased from Sinopharm Chemical Reagent Co., Ltd. (China); Oxoid Ltd. (UK); or Sigma-Aldrich Corporation (USA) unless otherwise stated. The enzymes for genetic manipulation were purchased from Thermo Fisher Scientific Co. Ltd. (USA) or Takara Biotechnology Co. Ltd. (China). Chemical reagents were purchased from standard commercial sources, including Sigma-Aldrich Corporation (USA), Merck KGaA (Germany). The bacterial strains, plasmids and primers used in this study are summarized in **Supplementary Tables 1** and **2**.

DNA Isolation, manipulation, and sequencing. DNA isolation and manipulation in *E. coli* or *Streptomyces* strains were carried out according to standard methods[42,43]. PCR amplifications were carried out on an Applied Biosystems Veriti Thermal Cycler either by Phanta Max Super-Fidelity DNA polymerase (Vazyme Biotech Co. Ltd., China) for routine genotype verification or by PrimeSTAR HS DNA polymerase (Takara Biotechnology Co., Ltd. Japan) for high-fidelity amplification. Primer synthesis was performed at Shanghai Sangon Biotech Co. Ltd. (China). DNA sequencing was conducted at Shanghai Majorbio Biotech Co. Ltd. (China).

Metabolite analysis. High performance liquid chromatography (HPLC) analysis was conducted on the Agilent 1200 HPLC system (Agilent Technologies Inc., USA) equipped with a DAD detector. Semipreparative HPLC was performed on an Agilent 1100 system. HPLC Electrospray ionization MS (HPLC-ESI-MS) was performed on the Thermo Fisher LTQ Fleet ESI-MS spectrometer (Thermo Fisher Scientific Inc., USA), and the data were analyzed using Thermo Xcalibur software. Optical rotations were measured on an Autopol-IV polarimeter from the sodium D line (590 nm). ECD spectra were recorded on a J-810 spectropolarimeter. High-resolution ESI-MS analysis was conducted on the 6230B Accurate Mass TOF LC/MS System (Agilent Technologies Inc., USA) and the data were analyzed using Agilent MassHunter Qualitative Analysis software. NMR data were recorded on the BrukerAvance III AV600 (Cryo) spectrometers (Bruker Co. Ltd., Germany) or on the Agilent ProPlus 500 MHz NMR spectrometer (Agilent Technologies Inc., USA).

Gene inactivation and complementation. The inactivation of each gene in *S. rugosporus* or *S. antibioticus* was performed by in-frame deletion or replacement to exclude polar effects on downstream gene expression. For in *trans* complementation, the target gene was under the control of *PermE**, the constitutive promoter for expressing the erythromycin-resistance gene in *Saccharopolyspora erythraea*. For details, please see **Supplementary Notes 1** and **2**.

Production and analysis of PYRs and intermediate 1. The fermentation was conducted according to a previously described method[9]. To analyze the product, 50 ml of each fermentation broth was extracted three times using an equal volume of EtOAc. After evaporation under reduced pressure to remove organic solvent, the residue was dissolved in methanol and subjected to HPLC analysis on an Agilent Zorbax column (SB-C18, 5 μm, 4.6 × 250 mm, Agilent Technologies Inc., USA) by gradient elution of mobile phase A (H_2O supplemented with 0.1% formic acid) and mobile phase B (acetonitrile supplemented with 0.1% formic acid) using a flow rate of 1 ml/min: 0–5 min, 10–30% phase B; 5–10 min, 30–65% phase B; 10–20 min, 65% phase B; 20–25 min, 65–100% phase B; 25–30 min, 100% phase B; and 30–35 min, 100–10% phase B (λ at 335 nm).

Production and analysis of CHL. Fifty microliters of spore suspension of each *S. antibioticus* strain was inoculated onto a plate containing 20 ml of solid medium (Soya meal 2%, D-mannitol 2%, 0.2% $CaCO_3$, Agar 2%) followed by incubation at 30 °C for 5 d. To analyze the product, the agar from each plate was chopped and extracted three times with 50 ml of methanol. Sonication was performed to improve the extraction efficiency. After filtration and evaporation under reduced pressure to remove organic solvent, the residue was dissolved in methanol and subjected to HPLC analysis, as described above for PYRs using the following program: 0–18 min, 30–100% phase B; 18–25 min, 100% phase B; 25–27 min, 100–30% phase B; and 27–30 min, 30% phase B (λ at 220 nm).

Protein expression and purification. The genes *pyrE3* and *pyrI4* from *S. rugosporus* and the genes *chlE3* and *chlL* from *S. antibioticus* were individually amplified by PCR using the corresponding primers, the sequences of which are presented in **Supplementary Table 2**. These PCR products were purified, digested with NdeI and HindIII (or NdeI and XhoI) and then ligated into the vector pET28a(+), which was digested with the same enzymes. The resulting recombinant plasmids, which are listed in **Supplementary Table 1**, were transferred into *E. coli* BL21(DE3) for protein overexpression. The culture of each *E. coli* transformant was incubated in Luria-Bertani (LB) medium containing 50 μg/ml kanamycin at 37 °C and at 250 r.p.m. until the cell density reached 0.6–0.8 at OD_{600}. Protein expression was induced by the addition of isopropyl-β-D-thiogalactopyranoside (IPTG) to a final concentration of 0.2 mM, followed by further incubation for 40 h at 16 °C. The cells were harvested by centrifuging at 5,000 r.p.m. for 20 min at 4 °C and were resuspended in 30 ml of lysis buffer (50 mM Tris-HCl, 300 mM NaCl, 10% glycerol, pH 7.0). After disruption by FB-110X Low Temperature Ultra-pressure Continuous Flow Cell Disrupter (Shanghai Litu Mechanical Equipment Engineering Co., Ltd, China), the soluble fraction was collected and subjected to purification of each target protein using a HisTrap FF column (GE Healthcare, USA). The desired protein fractions, as determined by SDS-PAGE, were concentrated and desalted using a PD-10 Desalting Column (GE Healthcare, USA) according to the manufacturer's protocols. The concentration of protein was determined by Bradford assay using bovine serum albumin (BSA) as the standard.

Site-specific mutation in PyrE3 and ChlE3. Rolling-cycle PCR amplification (using the primers listed in **Supplementary Table 2**) followed by subsequent DpnI digestion was conducted, according to the standard procedure of the QuikChange Site-Directed Mutagenesis Kit purchased from Stratagene (USA) or Mut Express II (Vazyme Biotech Co. Ltd, China). Each mutation was confirmed by sequencing. The resulting mutant proteins $PyrE3^{E32A}$ and $PyrE3^{D275A}$ or $ChlE3^{E32A}$ and $ChlE3^{D280A}$ were expressed in *E.coli* BL21(DE3), purified to homogeneity, and then concentrated according to the procedures described above for the native proteins.

Determination of the cofactor associated with PyrE3 and ChlE3. The UV spectra of the recombinant proteins PyrE3 and ChlE3 and their mutants were recorded at a concentration of 1 mg/ml on a Unico 4802 UV/Vis spectrophotometer (UNICO Instruments Co., Ltd., Shanghai). Each protein solution was incubated at 100 °C for 5 min for denaturation and then subjected to HR-ESI-MS analysis on a 6230B Accurate Mass TOF LC/MS System (Agilent Technologies Inc., USA) to examine the presence of FAD ($[M+H]^+$ *m/z* calcd. 786.1644; found 786.1589 from the PyrE3 sample and 786.1595 from the ChlE3 sample). The ECD spectra of PyrE3 and ChlE3 and their mutants were recorded (with a 1-nm bandwidth resolution and in 1-nm steps) in a 1-cm path length quartz cuvette at 25 °C using an AVIV 400 CD spectrophotometer (AVIV Biochemical, Inc., Lakewood, NJ) at a concentration of 0.2 mg/ml in 50 mM NaH_2PO_4 (pH 7.6) buffer. For scanning, the wavelength was varied from 190 nm to 300 nm.

Determination of the solubility in 50 mM Tris-HCl buffer (pH 7.0) containing 10% methanol for *in vitro* assays. A 50-mM methanol stock solution of each compound (**1**, **2** or **4**) was diluted (1: 10, v/v) using 50 mM Tris-HCl buffer (pH 7.0) and then incubated at 30 °C for 24 h. After centrifugation, the supernatant was subjected to HPLC analysis, which was performed on a reverse-phase column (Agilent Zorbax SB-C18 250 × 4.6 mm) by gradient elution of mobile phase A (H_2O supplemented with 0.1% formic acid) and mobile phase B (acetonitrile supplemented with 0.1% formic acid) with a flow rate of 1 ml/min: 0–5 min, 65% phase B; 5–15 min, 65–100% phase B; 15–20 min, 100% phase B; 20–25 min, 100–65% phase B; and 25–30 min, 65% phase B (λ at 280 nm). The solubility of each compound was determined according to the standard concentration curve, showing 0.86 ± 0.21 mM for **1**, 0.92 ± 0.27 mM for **4** and 0.68 ± 0.33 mM for **2**.

Conversion of compound 1 to 2 in *vitro*. The assays were conducted at 30 °C in a mixture containing 200 μM **1** in 50 mM Tris-HCl buffer (pH 7.0). PyrE3 and PyrI4 (or ChlE3 and ChlL), at a final concentration of 40 μM for each, were added to the solution to initiate the reaction (the total volume was 20 μl). After 15 min of incubation, the reactions were quenched by adding an equal volume of methanol. After centrifugation, the supernatant was subjected to HPLC or HPLC-ESI-MS analysis according the method described above.

Characterization of PyrE3-catalyzed dialkyldecalin formation in *vitro*. The assays were performed at 30 °C in mixtures containing 40 μM PyrE3 (or the

doi:10.1038/nchembio.1769

mutant protein, PyrE3^{E32A} or PyrE^{D275A}), 200 μM **1** and 10% methanol (v/v) in 50 mM Tris-HCl buffer (pH 7.5). The reaction in the absence of the enzyme was used as the negative control. The termination of the reactions and analysis of the resulting products were carried out according to the methods described above for PyrE3 and PyrI4-catalyzed conversion of **1** to **2**.

To evaluate the pH dependence of the PyrE3-catalyzed conversion of **1** to **4**, the reactions were performed at 30 °C for 1.0 min in 50 mM MES (pH 6.0 or 6.5) or 50 mM Tris-HCl (7.0, 7.5, 8.0, 8.5 or 9.0) buffer, in the presence of 0.33 μM PyrE3 and 200 μM **1**. The termination of each reaction and analysis of **1** consumption and **4** production were carried out according to the methods described above. These negative controls, product analysis methods and pH dependence assays were conducted as described here for the enzymes below unless indicated otherwise.

For kinetic analysis, a time-course experiment was conducted to determine the initial rate conditions. For this purpose, 0.33 μM PyrE3 was added to 20 μl of a reaction mixture that contained 200 μM compound **1** and 10% methanol in 50 mM Tris-HCl buffer (pH 7.5). The reactions were initiated by adding PyrE3, incubated at 30 °C and terminated by adding 20 μl of methanol at 0 min, 0.5 min, 1.0 min, 2.0 min, 5.0 min or 10.0 min. The samples were then subjected to HPLC analysis, as described above. The product yield was calculated according to the standard concentration curve of **4**. The production of **4**, which was linear with respect to time from 0 min to 1.0 min, was fitted to a linear equation to obtain the initial velocity. To determine the kinetic parameters for compound **1**, the PyrE3-catalyzed reactions were performed at 30 °C in solutions containing 0.33 μM PyrE3, 50 mM Tris-HCl buffer (pH 7.5), 10% methanol and varying concentrations of **1** (2.5 μM, 5 μM, 10 μM, 25 μM, 50 μM, 100 μM, 200 μM, 400 μM, 600 μM or 800 μM). All assays were performed in triplicate. The resulting initial velocities were then fitted to the Michaelis-Menten equation using OriginPro 8 (Originlab, Co., USA) extract the parameters K_m and k_{cat}.

Characterization of ChlE3-catalyzed dialkyldecalin formation in *vitro*. The assays were performed at 30 °C in mixtures containing 40 μM ChlE3 (or the mutant protein ChlE3^{E32A} or ChlE3^{D280A}), 200 μM **1** and 10% methanol in 50 mM Tris-HCl buffer (pH 7.5). The pH dependence was determined as described above, except that the reactions were performed for 2 min. For kinetic analysis, a time-course experiment was conducted to determine the initial rate conditions in each 20 μl reaction mixture that contained 200 μM **1**, 5 μM ChlE3 and 10% methanol in 50 mM Tris-HCl buffer (pH 7.5). The reactions were initiated by adding ChlE3 and incubated at 30 °C and then terminated with 20 μl of methanol at 0 min, 0.5 min, 1.0 min, 2.0 min, 5.0 min or 10.0 min. The samples were then subjected to HPLC analysis, as described above. The production of **4**, which was linear with respect to time from 0–2.0 min, was fitted to a linear equation to obtain the initial velocity. To determine the kinetic parameters for compound **1**, the reactions were performed at 30 °C in solutions containing 5 μM ChlE3, 10% methanol, 50 mM Tris-HCl buffer (pH 7.5) and varying concentrations of **1** (5 μM, 10 μM, 25 μM, 50 μM, 100 μM, 200 μM, 400 μM or 800 μM,). All assays were performed in triplicate. The extraction of the K_m and k_{cat} parameters was conducted as described above.

Characterization of PyrI4-catalyzed spiro-conjugate formation in *vitro*. The assays were performed at 30 °C in mixtures containing 40 μM PyrI4, 200 μM compound **4** and 10% methanol in 50 mM Tris-HCl buffer (pH 7.5). To exclude metal ion dependence, the reaction was conducted after the addition of 1 mM ethylene diamine tetraacetic acid (EDTA). For kinetic analysis, a time-course experiment was conducted to determine the initial rate conditions in each 20-μl reaction mixture that contained 200 μM **4**, 0.3 μM PyrI4 and 10% methanol in 50 mM Tris-HCl buffer (pH 7.5). The reactions were initiated by adding PyrI4, incubated at 30 °C and then terminated with 20 μl of methanol at 0 min, 0.5 min, 1.0 min, 2.0 min, 5.0 min or 10.0 min. The production of **2**, which was linear with respect to time from 0–1.0 min, was fitted to a linear equation to obtain the initial velocity. To determine the kinetic parameters of **4**, reactions were performed at 30 °C in the solutions containing 0.3 μM PyrI4, 10% methanol, 50 mM Tris-HCl buffer (pH 7.5) and varying concentrations of **4** (0 μM, 25 μM, 50 μM, 100 μM, 200 μM, 400 μM, 600 μM or 800 μM). All assays were performed in triplicate. The extraction of the K_m and k_{cat} parameters was conducted as described above.

Characterization of ChlL-catalyzed spiro-conjugate formation in *vitro*. The assays were performed at 30 °C in mixtures containing 40 μM ChlL, 200 μM **4** and 10% methanol in 50 mM Tris-HCl buffer (pH 7.0). The pH dependence was determined as described above, except that the reactions were performed for 5 min. For kinetic analysis, a time-course experiment was conducted to determine the initial rate conditions in each 20-μl reaction mixture that contained 200 μM **4**, 20 μM ChlL and 10% methanol in 50 mM Tris-HCl buffer (pH 7.0). The reactions were initiated by adding ChlL, incubated at 30 °C and then terminated with 20 μl of methanol at 0 min, 0.5 min, 1.0 min, 2.0 min, 5.0 min or 10.0 min. The production of **2**, which was linear with respect to time from 0–5.0 min, was fitted to a linear equation to obtain the initial velocity. To determine the kinetic parameters of **4**, reactions were performed at 30 °C in the solutions containing 20 μM ChlL, 10% methanol, 50 mM Tris-HCl buffer (pH 7.0) and varying concentrations of **4** (25 μM, 50 μM, 100 μM, 200 μM, 400 μM, 600 μM or 800 μM). All assays were performed in triplicate. The extraction of the K_m and k_{cat} parameters was conducted as described above.

Compound isolation and purification. Compound **1** was produced as the intermediate by the corresponding Δ*pyrE3* mutant *S. rugosporus* strain, whereas **2** or **4** accumulated upon scale-up of the *in vitro* reaction catalyzed by both PyrE3 and PyrI4 (for **2**) or by PyrE3 alone (for **4**). Compound **3** was prepared by hydrolysis of the PYRs isolated from the wild-type *S. rugosporus* strain.

For **1**, 120 l of the culture broth of the Δ*pyrE3 S. rugosporus* mutant strain was extracted with EtOAc. The EtOAc extract was fractionated by octadecylsilyl column chromatography (LiChroprep RP-18, 40–63 μm, Merck KGaA, Germany), using a gradient elution of methanol in H_2O (30–100%). The **1**-containing product was further fractionated by semipreparative HPLC (on an Agilent Zorbax SB-C18 column, 9.4 × 250 mm, 75% acetonitrile supplemented with 0.1% formic acid, 4 ml/min, λ at 220 nm), followed by freeze-drying to yield **1** (13.4 mg).

Compound **2** was prepared by scale-up of the PyrE3 and PyrI4-catalyzed conversion of **1**. The reaction proceeded at 30 °C in a 20-ml mixture containing 3.5 mg of **1**, 5% methanol, 50 μM PyrE3, and 50 μM PyrI4 in 50 mM Tris-HCl buffer (pH 7.0). After completion of the reaction, the reaction mixture was extracted three times with EtOAc (20 ml for each). The organic extracts were concentrated under reduced pressure, and the crude residue was subjected to semi-preparative HPLC (70% acetonitrile supplemented with 0.1% formic acid, 4 ml/min, λ at 220 nm) to yield **2** (2.0 mg, 57% yield).

Compound **3**, the aglycone of PYRs, was obtained by acid hydrolysis of the PYRs isolated from the wild-type *S. rugosporus* strain. Ten liters of the culture broth of *S. rugosporus* was extracted with EtOAc to afford the crude residue (8.0 g). The extract was fractionated by octadecylsilyl column chromatography to afford PYRs using an elution program with a gradient of methanol in H_2O (10–100%). The PYR-containing fractions were then subjected to acid hydrolysis with 0.5 M CF_3COOH in 10% methanol at 60 °C for 1 h. The hydrolysate was separated by semipreparative HPLC (45% acetonitrile supplemented with 0.1% formic acid, 4 ml/min, λ at 220 nm) to yield **3** (5.7 mg).

Compound **4** was produced by scaling-up the PyrE3-catalyzed conversion of **1**. The reaction proceeded at 30 °C in a 40-ml mixture containing 4.5 mg of **1**, 5% methanol and 50 μM PyrE3 in 50 mM Tris-HCl buffer (pH 7.0). After incubating for 30 min, the reaction mixture was extracted three times with EtOAc (40 ml for each). The combined organic layers were concentrated under reduced pressure. The crude residue was subjected to semi-preparative HPLC (λ at 220 nm) using a gradient elution of mobile phase A (H_2O supplemented with 0.1% formic acid) and phase B (acetonitrile with 0.1% formic acid) with a flow rate of 4 ml/min: 0–5 min, 65% phase B; 5–15 min, 65–100% phase B; 15–20 min, 100% phase B, to yield **4** (3.1 mg, 66% yield).

Computational analysis. Mixed torsional/low mode conformational analyses were conducted with the Macromodel 9.9.223 software (MacroModel, Schrödinger LLC, 2012; http://www.schrodinger.com/productpage/14/11/), using Merck Molecular Force Field (MMFF) with an implicit solvent model for methanol in a 21 kJ/mol energy window. Geometry reoptimizations of the resulting conformers (using B3LYP/6-31G(d) level *in vacuo* and B97D/TZVP with PCM solvent model for methanol) and TDDFT-ECD calculations were performed with Gaussian 09 (ref. 44) using various functionals (B3LYP, BH&HLYP and PBE0) and the TZVP basis set. ECD spectra were generated as the sum of Gaussians[45] with a 2,700 cm^{-1} half-height width (corresponding to ~27 at 320 nm), using dipole-velocity computed rotational strengths. Boltzmann distributions were estimated from the ZPVE-corrected B3LYP/6-31G(d) energies in the gas-phase calculations and from the B97D/TZVP

energies in the PCM model ones. The MOLEKEL[46] software package was used for visualization of the results.

Homology modeling of flavoenzymes. Computational modeling of PyrE3 and ChlE3 was performed using the protein structure prediction platform I-TASSE (http://zhanglab.ccmb.med.umich.edu/I-TASSER)[47]. The computational models of PyrE3 and ChlE3 on the basis of the major structural analog OxyS (Protein Data Bank code 4K2X, 41% identity to PyrE3 and 42% identity to ChlE3) presented C-scores of 1.21 and 1.52 for PyrE3 and ChlE3, respectively, which indicates high confidence in the model accuracy (C-score >−1.5). Potential residues binding with FAD were suggested as computational predictions.

42. Green, M.R. & Sambrook, J. *Molecular Cloning: a Laboratory Manual* 4th edn. (Cold Spring Harbor Laboratory Press, 2012).
43. Keiser, T., Bibb, M.J., Buttner, M.J., Chater, K.F. & Hopwood, D.A. *Practical Streptomyces Genetics* (John Innes Foundation, 2000).
44. Frisch, M.J. *et al. Gaussian 09, Revision B.01* (Gaussian, Inc., Wallingford CT, 2010).
45. Stephens, P.J. & Harada, N. ECD Cotton effect approximated by the Gaussian curve and other methods. *Chirality* **22**, 229–233 (2010).
46. Varetto, U. *MOLEKEL 5.4.* (Swiss National Supercomputing Centre: Manno, Switzerland, 2009).
47. Roy, A., Kucukural, A. & Zhang, Y. I-TASSER: a unified platform for automated protein structure and function prediction. *Nat. Protoc.* **5**, 725–738 (2010).

doi:10.1038/nchembio.1769